Frequency conversion and amplification of photon-number detection

G. M. D'Ariano* and C. Macchiavello†

Dipartimento di Fisica "Alessandro Volta" Università degli Studi di Pavia via A. Bassi 6, I-27100 Pavia, Italy

(Received 14 April 1993)

We present a comparative analysis of trilinear parametric processes for photon-number detection. Attention is focused on those processes that correspond to constituent devices in optical networks, such as second- and subharmonic sum- and difference-frequency generation and phase-sensitive and insensitive amplification and attenuation. Gains, output Fano factors, and noise figures are given for input in both coherent and number eigenstates. The fully quantum processes (i.e., with no classical pump) are evaluated numerically. It is shown that the depletion of the quantum pump is never complete and this accounts for additional noise at the output. Second-harmonic and sum-frequency generation turn out to be more efficient and less noisy than the respective down-conversion processes. Ideal behaviors are also reported for comparison and the results are discussed with a brief parallel analysis of the various devices.

PACS number(s): 42.50.Dv, 42.65.Ky, 42.79.Nv

I. INTRODUCTION

Nonlinear optical processes have attracted much attention in recent years, mostly in view of the potentially unlimited spectrum of nonclassical features that can be exhibited (see, for example, Ref. [1] and references quoted therein). Processes with multilinear Hamiltonians in field operators also describe the basic dynamics of all building-block devices in optical networks and thus are interesting for analyzing the ultimate network performance in the quantum-limited regime. Simple models of amplifiers, both analytical [2–4] and numerical [5] have been studied, whereas the bases of the quantum communication and detection theory have been established [6]. However, a thorough analysis of many nonlinear devices is still lacking, mostly due to the computational effort needed for evaluating the field dynamics in the truly quantum case.

The simplest nonlinear processes that describe a wide class of optical devices are the parametric trilinear ones, as, for example, second- and subharmonic and sum- and difference-frequency generation. Here the term *parametric* is used to denote those nonlinear processes that involve only nonresonant (i.e., virtual) excitations of the medium, and hence satisfy the Manley-Rowe relations. Conversely, those processes that involve resonant transitions at the frequencies of the medium are termed *nonparametric* (see Ref. [7] for anomalies in this classification). The parametric processes involve only photon (i.e., boson) operators in the effective interaction Hamiltonian, whereas the nonparametric ones involve also matter (i.e., fermion) degrees of freedom. In this sense the laser transition itself and the stimulated Raman scattering are examples of nonparametric processes.

Depending on the input state of the field modes involved in the process, the same multilinear Hamiltonians lead either to amplification or to frequency conversion. In the parametric amplifier there is a classical highly excited pump, which essentially remains undepleted during the process, whereas a signal mode, which initially carries the input photons, gains many additional photons during the process. A third *idler* mode is also needed for matching frequencies: this mode is initially empty and gets some photons at the output, which become the main source of added noise for the amplifier. Frequency conversion occurs when some initially empty modes are filling up with photons, to the detriment of a depleting quantum pump. (Eventually an additional classical pump can be considered in order to have more freedom in choosing frequencies.) Notice that the total number of photons is generally not conserved: one has instead constants of motion in the form of linear combinations of the photon numbers of the modes with integer coefficients. These conserved quantities are the quantum analog of the Manley-Rowe relations. Nonconservation of the total photon number leads to amplification or attenuation of the photon number also in the case of frequency conversion.

The performance of the optical device is conveniently described by the (effective) gain $\mathcal{G}$ and the noise figure $\mathcal{R}$,

$$\mathcal{G} = \frac{\mathcal{S}_{\text{out}}}{\mathcal{S}_{\text{in}}}, \qquad \mathcal{R} \equiv \frac{(\mathcal{S}^2/\mathcal{N})_{\text{in}}}{(\mathcal{S}^2/\mathcal{N})_{\text{out}}}. \qquad (1)$$

Typically, for on-off modulation $\mathcal{S}_{\text{in}}$ denotes the peak ensemble average $\langle \hat{O} \rangle$ of the detected observable $\hat{O}$ at the input, $\mathcal{S}_{\text{out}}$ is the difference between the output mean values in the presence and absence of input, and $\mathcal{N} \equiv \langle \Delta \hat{O}^2 \rangle$ represents the noise. $\mathcal{G} < 1$ describes attenuation. In the ideal case the device is linear and noiseless, namely, $\mathcal{G}$ does not depend on $\mathcal{S}_{\text{in}}$ and the noise figure is minimum, i.e., $\mathcal{R} = 1$. For real devices $\mathcal{G}$ and $\mathcal{R}$ depend in general on both the input state and on the particular detection scheme. In practice, for input coherent states and any kind of detection the minimum attainable noise figure is $\mathcal{R} \simeq 2$ (namely, 3 dB) for optical derivations and conventional amplifiers [8, 9].

For direct detection ($\hat{O} = \hat{n}$) the noise figure is meaningless when using input number eigenstates: in this case the performance of the device can be described by the output Fano factor $\mathcal{F}_{\text{out}}$, where

$$\mathcal{F} = \frac{\langle \Delta \hat{n}^2 \rangle}{\langle \hat{n} \rangle} \ . \tag{2}$$

We remark that the ultimate performance of an optical network is basically limited by noise of quantum origin, which arises at the detection stage as the signature of the Heisenberg uncertainty principle and makes all the noise figures depend on both the detection mode and the radiation state. Apart from technical reasons, which may suggest a particular detection scheme (direct, homodyne, or heterodyne) depending on the actual performances of the currently available devices, in the ideal limit the best operation is attained using direct detection and coding information on number eigenstates. In fact, number eigenstates achieve the channel capacity of the field and allow complete reduction of the bit-error rate without the need of increasing the power along the line. Moreover, due to their peculiar property of being an orthogonal set, they also allow photon duplication (ideal photon splitting), a tool suited to attain perfect optical transceivers [10–15].

In this paper we present an analysis for direct detection with coherent and number input states, of the parametric trilinear Hamiltonians corresponding to second- and subharmonic and sum- and difference-frequency generation. We analyze separately the various cases describing different devices: phase-sensitive and -insensitive amplifiers or attenuators and frequency-converting devices. In the fully quantum cases we solve the dynamics numerically through block diagonalization of the Hamiltonians. The results are schematically presented in the form of plots for gains, noise figures, and output Fano-factors, comparing them with the corresponding ideal behavior.

II. ANALYSIS OF THE TRILINEAR PARAMETRIC PROCESSES

The trilinear parametric processes are described by the effective interaction Hamiltonian

$$\hat{H} = \kappa \left(ab^\dagger c^\dagger + a^\dagger bc \right) \ . \tag{3}$$

The coupling κ is the nonlinear second-order susceptibility $\chi^{(2)}$ of the medium at the given frequencies and $\omega_a = \omega_b + \omega_c$. Also a third-order susceptibility $\chi^{(3)}$ can correspond to an effective Hamiltonian of the trilinear form (3) when the fourth mode at frequency ω_p is a classical pump which remains essentially undepleted during the process (such approximation of classical undepleted pump is also usually referred to as *paramet-*

ric). In this case $\kappa = \chi^{(3)} \sqrt{I_p}$, I_p being the pump intensity, whereas the frequencies now satisfy the relation $\omega_a - \omega_b - \omega_c = \pm \omega_p$. Using a $\chi^{(3)}$ process—instead of a $\chi^{(2)}$—may be convenient in practice because the $\chi^{(2)}$ susceptibility is zero for cubic symmetry, and thus materials with sizeable $\chi^{(3)}$ are more commonly available. Moreover, the pump mode allows more freedom for matching wave vectors and frequencies of the modes in the medium, and can be used to tune the coupling κ and the relative phases between the modes. (The pump mode, however, should be kept very stable with respect to the other modes.)

For degenerate b and c, the Hamiltonian (3) takes the form

$$H = \kappa \left(ab^{\dagger^2} + a^\dagger b^2 \right) \ , \tag{4}$$

whereas when one of the three modes is classical undepleted the Hamiltonian becomes effectively bilinear. In Table I all the possible trilinear parametric processes are summarized. The processes differ from each other either in initial conditions or in the eventual occurrence of a classical pump. In the following we analyze in detail all the devices corresponding to such processes: the three-wave mixing processes (with all the modes a, b, and c initially nonvacuum) are not considered, as they do not correspond to elementary optical devices.

A. Phase-sensitive amplifier

When mode a in the Hamiltonian (4) can be considered as a classical pump, one obtains a generation of squeezed states in b, starting from coherent input. The corresponding amplifier is the so-called *phase-sensitive* amplifier, with effective Hamiltonian

$$\hat{H} = \kappa \left(b^2 + b^{\dagger^2} \right) \ . \tag{5}$$

The coupling constant now is $\kappa = \chi^{(2)} \sqrt{I_a}$. All quantities can be analytically evaluated from the evolution of the field in a medium of length L

$$b \longrightarrow \cosh(2\kappa L)b + \sinh(2\kappa L)b^\dagger \ . \tag{6}$$

For input number state $|n\rangle$ the following gain and output Fano factor are obtained:

$$\mathcal{G} = \cosh(4\kappa L) \ , \tag{7}$$

TABLE I. Summary of parametric trilinear processes for direct detection (three-wave mixing is not considered).

Process	$\langle \hat{n}_a \rangle_{\text{in}}$	$\langle \hat{n}_b \rangle_{\text{in}}$	$\langle \hat{n}_c \rangle_{\text{in}}$	$\mathcal{S}_{\text{in}}$	$\mathcal{S}_{\text{out}}$
Phase-sensitive amplifier	Classical	$\neq 0$		$\langle \hat{n}_b \rangle_{\text{in}}$	$\langle \hat{n}_b \rangle_{\text{out}}$
Subharmonic generation	0	$\neq 0$		$\langle \hat{n}_b \rangle_{\text{in}}$	$\langle \hat{n}_a \rangle_{\text{out}}$
Second-harmonic generation	$\neq 0$	0		$\langle \hat{n}_a \rangle_{\text{in}}$	$\langle \hat{n}_b \rangle_{\text{out}}$
Phase-insensitive amplifier	Classical	$\neq 0$	0	$\langle \hat{n}_b \rangle_{\text{in}}$	$\langle \hat{n}_b \rangle_{\text{out}} - (\mathcal{G} - 1)$
Simple frequency conversion	$\neq 0$	0	Classical	$\langle \hat{n}_a \rangle_{\text{in}}$	$\langle \hat{n}_b \rangle_{\text{out}}$
Difference-frequency generation	$\neq 0$	0	0	$\langle \hat{n}_a \rangle_{\text{in}}$	$\langle \hat{n}_b \rangle_{\text{out}} = \langle \hat{n}_c \rangle_{out}$
Sum-frequency generation	0	$\neq 0$	$\neq 0$	$\langle \hat{n}_b \rangle_{\text{in}} = \langle \hat{n}_c \rangle_{\text{in}}$	$\langle \hat{n}_a \rangle_{\text{out}}$

$$\mathcal{F}_{\text{out}} = \frac{1}{2} \frac{\sinh^2(4\kappa L)\left(n^2 + n + 1\right)}{\cosh(4\kappa L)n + \sinh^2(2\kappa L)} . \tag{8}$$

The gain is exponentially increasing versus pump intensity (in practice it is unlimited as long as the signal is much less intense than the pump). The Fano factor increases versus input signal and is asymptotically linear for large signals. Such enhanced noise is due to the fact that this amplifier is sensitive to the phase of the signal, and thus works very inefficiently with phaseless states like the number eigenstates. On the contrary, it is well adapted to input coherent states, with gain strongly dependent on the phase of the input relative to that of the pump. When both are in phase the maximum gain is obtained,

$$\mathcal{G} = \exp(4\kappa L) , \tag{9}$$

whereas when in quadrature the amplifier actually works as an attenuator, with gain

$$\mathcal{G} = \exp(-4\kappa L) . \tag{10}$$

For both cases (9) and (10) the noise figure is given by

$$\mathcal{R} = 1 + \frac{\left(1 - \mathcal{G}^{-2}\right)^2}{8\mathcal{S}_{\text{in}}} , \tag{11}$$

where $\mathcal{S}_{\text{in}}$ is the average photon number of the input coherent state. For large κL the gain (9) for coherent input is almost twice that for number eigenstates. With coherent inputs the noise figure approaches the ideal unit value asymptotically for large input signals, both in the amplifying and attenuating cases. In Sec. III the above features will be compared with those of other parametric devices and with the ideal cases.

B. Second- and subharmonic generation

These processes are described by the Hamiltonian (4). In particular, second-harmonic generation $\omega_b \to \omega_a$ corresponds to $\langle n_a \rangle_{\text{in}} = 0$, and the number of photons created at ω_a is equal to half the photons annihilated at ω_b. Conversely, subharmonic generation $\omega_a \to \omega_b$ corresponds to $\langle n_b \rangle_{\text{in}} = 0$ and the number of photons created at ω_b is twice those annihilated at ω_a.

The Hamiltonian (4) has the following constant of motion:

$$2\hat{n}_a + \hat{n}_b = \hat{C} , \tag{12}$$

which splits the Hilbert space into subspaces corresponding to fixed eigenvalues C of $\hat{C}$. These subspaces are spanned by the vectors

$$|n\rangle_C = |n, C - 2n\rangle , \qquad n = 0, 1, \ldots, [C/2] , \tag{13}$$

where $[x]$ denotes the integer part of x. In the basis (13) the Hamiltonian (4) takes the tridiagonal form

$$\hat{H}|n\rangle_C = h_n^{(C)}|n - 1\rangle_C + h_{n+1}^{(C)}|n + 1\rangle_C , \tag{14}$$

$$h_n^{(C)} = \sqrt{n(C - 2n + 1)(C - 2n + 2)} , \tag{15}$$

which is suited to numerical diagonalization.

The performance of the two processes has been analyzed through numerical diagonalization of the block Hamiltonians (15) (as a check, some numerical results presented in Ref. [16] have been reproduced). A sample of the evolution of the output signal and noise for source mode in a number eigenstate is given in Fig. 1, for initial photon number $n_{\text{in}} = 20$. By varying n_{in} one could see that the time dependence is periodic or quasiperiodic for very low n_{in}, whereas it becomes more and more irregular and irreversible for increasing n_{in} [17]. Qualitative differences between subharmonic and second-harmonic generation are evident. In the former the output signal exhibits maxima corresponding to a high noise level, and low noise occurs only for a depleted signal. In the latter, on the contrary, the first occurrence of a local maximum of the output signal coincides with the absolute maximum, and the corresponding noise is always well below all the subsequent values (and decreases versus n_{in}). Conversion is never complete in both cases; however, it is more efficient for second-harmonic than for subharmonic generation, due to the low noise at the output. The conversion length L_c has been identified as that corresponding to the first local maximum of the signal: a quantum mean-field approach [17] leads to a dependence $L_c \sim (1/2\kappa) n_{\text{in}}^{-1/2} \ln n_{\text{in}}$, in agreement with the numerical evaluation.
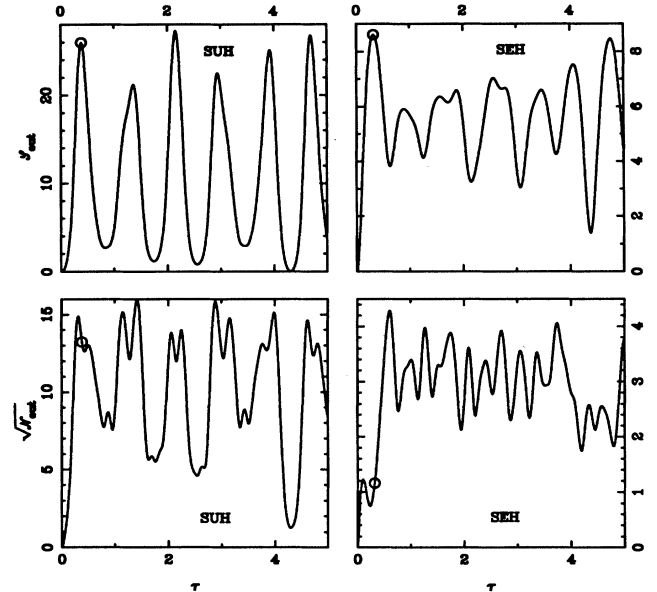

FIG. 1. Time evolution of output signal $\mathcal{S}_{\text{out}}$ and noise $\mathcal{N}_{\text{out}}$ for parametric subharmonic and second-harmonic generation [Hamiltonian (4)]. In all plots the input state of the source mode is a number eigenstates with $n = 20$. Circles enclose the conversion point. (Legend: SUH, subharmonic generation; SEH, second-harmonic generation; SUM, sum-frequency generation; DIF, difference-frequency generation; PIA, phase-insensitive amplifier; PSA, phase-sensitive amplifier.)

The gains at the conversion length L_c are plotted in Fig. 2 for the source mode in a number eigenstate. Subharmonic generation exhibits a gain $\mathcal{G}$ which decreases as a function of the input signal, and approaches the value $\mathcal{G} \simeq 1.28$ for large signals, well below the ideal gain $\mathcal{G} = 2$. The corresponding Fano factor increases as a function of the input signal with an almost linear behavior (this is not evident from Fig. 2 due to the semilog plot). Second-harmonic generation is much more efficient than subharmonic generation: the gain achieves asymptotically the ideal value $\mathcal{G} = \frac{1}{2}$ for large input signals, and the Fano factor tends to $\mathcal{F}_{\text{out}} = 0.13$.

In Fig. 3 the gain and the noise figure are plotted for the coherent source. Regarding the gain, the same considerations made for the previous case of the source in a number eigenstate hold. From the plot of the noise figure, however, it is now more evident that subharmonic generation is very noisy, whereas second-harmonic gener-

ation can achieve a noise figure lower than the customary 3-dB threshold (however, higher than the ideal noise figure). Plots corresponding to other devices operating at the same gain are given in the same figures for comparison: these will be discussed in Sec. III.

C. Phase-insensitive amplifier

With the mode a as a classical undepleted pump the interaction Hamiltonian (3) becomes

$$\hat{H} = \kappa \left(b^{\dagger} c^{\dagger} + bc \right) . \tag{16}$$

The Hamiltonian (16) describes the usual parametric amplifier when one of the difference-frequency modes—the signal mode, say b—is initially undepleted, whereas the other mode c—the idler—is initially depleted. From the Hamiltonian (16) one obtains the evolution of the field
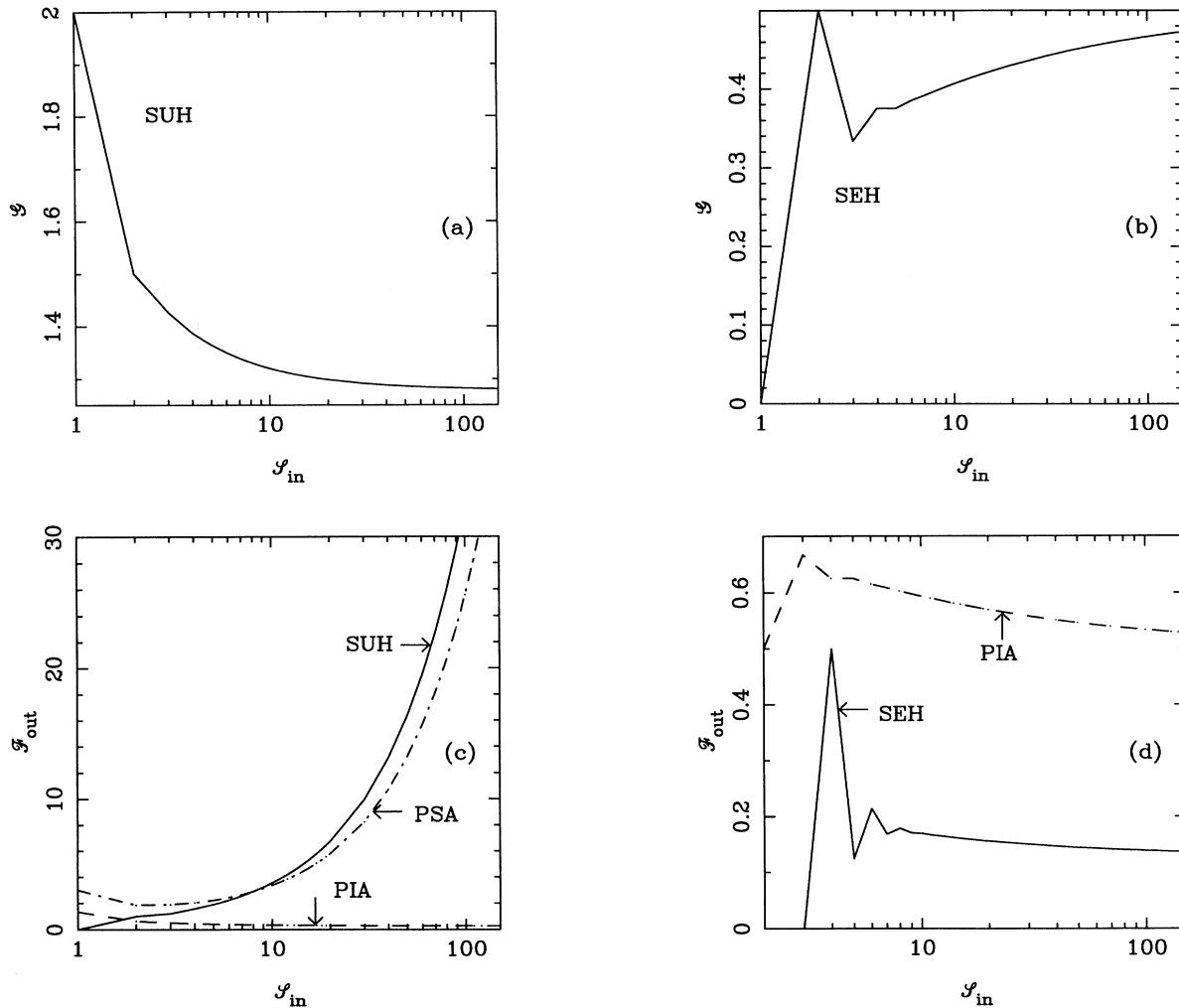

FIG. 2. Gain $\mathcal{G}$ and output Fano factor $\mathcal{F}_{\text{out}}$ for parametric subharmonic and second-harmonic generation [Hamiltonian (4)]. Comparison with other devices operating at the same gain $\mathcal{G}$ (see legend in Fig. 1). In all figures the input state is a number eigenstate; plotted lines are meaningful only for integer values of the abscissa.

modes

$$b_{\text{out}} = \mathcal{G}^{1/2} b_{\text{in}} + (\mathcal{G} - 1)^{1/2} c_{\text{in}}^{\dagger} \, ,$$

$$c_{\text{out}} = (\mathcal{G} - 1)^{1/2} b_{\text{in}}^{\dagger} + \mathcal{G}^{1/2} c_{\text{in}} \, ,$$

$$(17)$$

where the gain $\mathcal{G}$ is given by

$$\mathcal{G} = \cosh^2(\kappa L) \, , \qquad (18)$$

for interaction length L. (In evaluating the gain one should keep in mind that the incoherent threshold $\mathcal{G} - 1$ for zero input has to be subtracted from the output level $\langle b^{\dagger} b \rangle_{\text{out}}$.) The amplifier is linear, namely, the effective gain $\mathcal{G}$ does not depend on the input signal. From Eqs. (17) one also obtains the evolution of the noise,

$$\mathcal{N}_{\text{out}} \equiv \langle \Delta \hat{n}_b^2 \rangle_{\text{out}} = \mathcal{G} \langle \hat{n}_b \rangle_{\text{in}} + (\mathcal{G} - 1) \langle \hat{n}_c + 1 \rangle_{\text{in}} + 2\mathcal{G}(\mathcal{G} - 1) \langle \hat{n}_b \rangle_{\text{in}} \langle \hat{n}_c + 1 \rangle_{\text{in}} + (\mathcal{G} - 1)^2 \langle 2\hat{n}_c + 1 \rangle_{\text{in}}$$

$$+ \mathcal{G}^2 \langle \hat{n}_b \rangle_{\text{in}} [(\mathcal{F}_b)_{\text{in}} - 1] + (\mathcal{G} - 1)^2 \langle \hat{n}_c \rangle_{\text{in}} [(\mathcal{F}_c)_{\text{in}} - 1] + \mathcal{G}(\mathcal{G} - 1) \left[\langle b^{\dagger^2} \rangle_{\text{in}} \langle c^{\dagger^2} \rangle_{\text{in}} + \text{H.c.} \right] \, . \qquad (19)$$
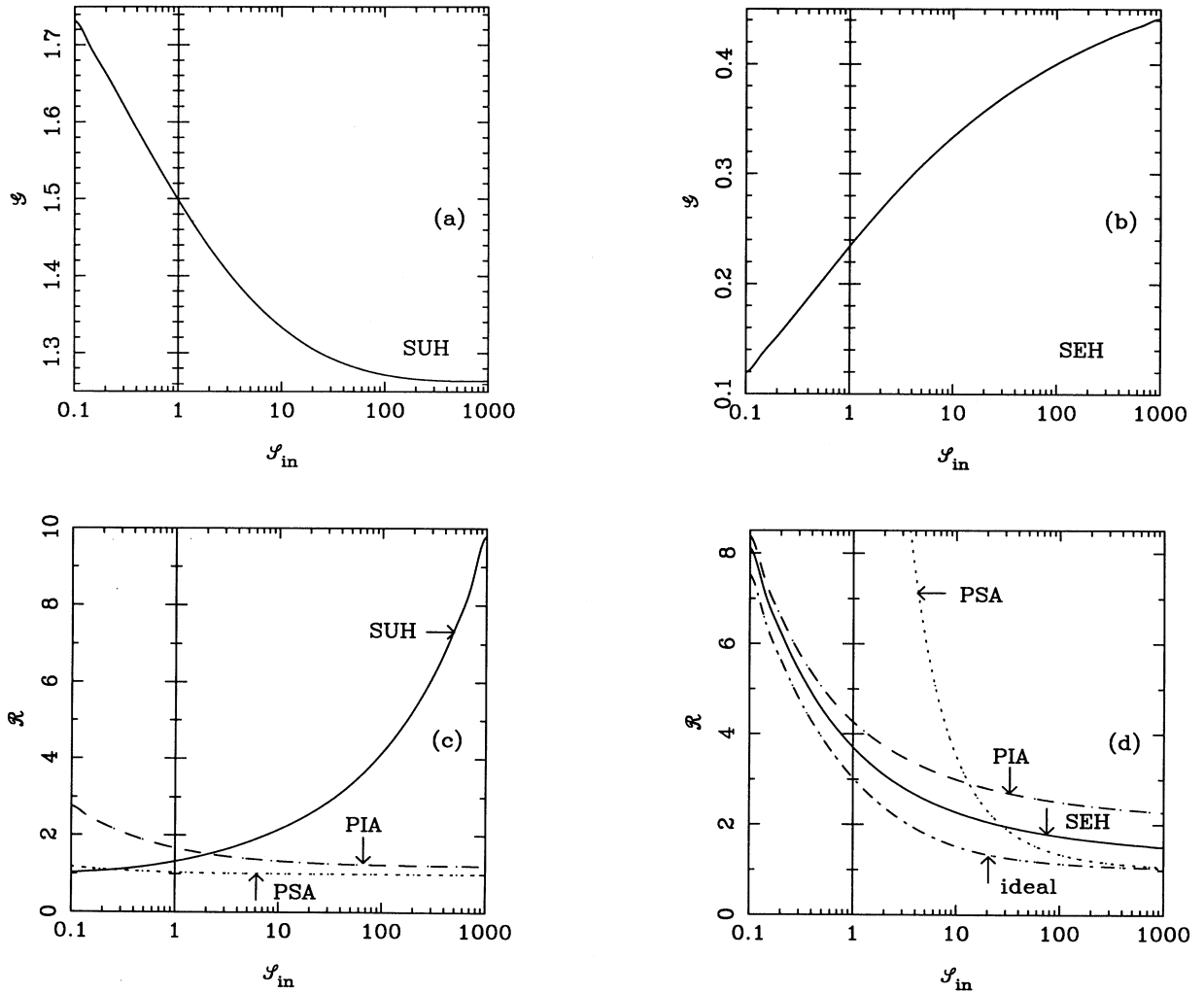

FIG. 3. Gain $\mathcal{G}$ and noise figure $\mathcal{R}$ for parametric subharmonic and second-harmonic generation, for input coherent states at the source mode. Comparison with other devices operating at the same gain and with ideal behavior (see legend in Fig. 1). The ideal limits are evaluated according to the analytical results given in Refs. [10–12].

The various contributions to the noise are usually referred to as [following the same order in Eq. (19)]: (i) quantum fluctuations of the amplified signal; (ii) amplified parametric spontaneous emission (the first two terms are the so-called shot noise [2]); (iii) quantum beat between the first and second terms; (iv) self-beat of parametric spontaneous emission; (v) excess noise of the signal and (vi) of the idler; (vii) coherent terms. For the vacuum idler $\langle \hat{n}_c \rangle_{\text{in}} = 0$ and large input signals $\langle \hat{n}_b \rangle_{\text{in}} \gg \mathcal{G}$ one has the asymptotic noise figure

$$\mathcal{R} \simeq 1 + \frac{\mathcal{G}-1}{\mathcal{G}(\mathcal{F}_b)_{\text{in}}} \,, \tag{20}$$

which for coherent inputs and large gains $\mathcal{G} \gg 1$ leads to the customary 3-dB threshold due only to the term (iii). A comparison with the characteristics of the other devices is discussed in Sec. III.

The same performance of the phase-insensitive amplifier can be obtained with a two level-medium nonparametric amplifier, as, for example, an erbium-doped active amplifier. In a simple two-level-atom model, which does not take into account saturation effects (this approximation is analogous to that of undepleted pump for the parametric amplifier), the noise still has a form very similar to Eq. (19), but now with the spontaneous emission playing the role of the idler mode.

D. Simple conversion between two frequencies (attenuation)

When mode c is a classical pump, the interaction Hamiltonian (3) is equivalent to the following:

$$\hat{H} = \kappa \left(a^\dagger b + a b^\dagger \right) \,, \tag{21}$$

with $\kappa = \chi^{(2)}\sqrt{I_c}$. Such a Hamiltonian is that of an ideal frequency converter between two modes (ideal processes are treated in Refs. [10–12]). Ideal conversion between two frequencies can thus be attained in practice only by using a trilinear process with a very strong pump. The conversion length is $L_c = \frac{\pi}{2\kappa}$. For generic length $L \neq L_c$ Hamiltonian (21) leads to linear attenuation of the photon number, with gain

$$\mathcal{G} = \cos^2(Lk) \leq 1 \,. \tag{22}$$

The device converts the signal towards higher frequencies when the source mode is b (and conversely when the source is a). The present device could also be viewed as a completely passive one—as, for example, in the case of a beam splitter—with no pump mode c and no frequency change from a to b.

The evolution of the field modes is

$$a_{\text{out}} = \mathcal{G}^{1/2} a_{\text{in}} + (1-\mathcal{G})^{1/2} b_{\text{in}} \,,$$

$$b_{\text{out}} = -(1-\mathcal{G})^{1/2} a_{\text{in}} + \mathcal{G}^{1/2} b_{\text{in}} \,. \tag{23}$$

From Eqs. (23) one obtains the output noise

$$\mathcal{N}_{\text{out}} \equiv \langle \Delta \hat{n}_a^2 \rangle_{\text{out}} = \mathcal{G}\langle \hat{n}_a \rangle_{\text{in}} + (1-\mathcal{G})\langle \hat{n}_b \rangle_{\text{in}} + 2\mathcal{G}(1-\mathcal{G})\langle \hat{n}_a \rangle_{\text{in}}\langle \hat{n}_b \rangle_{\text{in}}$$

$$+ \mathcal{G}^2 \langle \hat{n}_a \rangle_{\text{in}}[(\mathcal{F}_a)_{\text{in}} - 1] + (1-\mathcal{G})^2 \langle \hat{n}_b \rangle_{\text{in}}[(\mathcal{F}_b)_{\text{in}} - 1] + \mathcal{G}(1-\mathcal{G})\left[\langle a^{\dagger^2} \rangle_{\text{in}}\langle b^{\dagger^2} \rangle_{\text{in}} + \text{H.c.}\right] \,. \tag{24}$$

The various contributions are similar to those for the amplifying case in Eq. (19). Noise is minimized for $\langle \hat{n}_b \rangle_{\text{in}} = 0$. For large signals the noise-figure becomes

$$\mathcal{R} \simeq 1 + \frac{1-\mathcal{G}}{\mathcal{G}(\mathcal{F}_a)_{\text{in}}} \,, \tag{25}$$

which for $\mathcal{G} = 1/2$ (for example, a 50-50 beam splitter) and coherent input leads to the customary 3-dB degradation. Comparisons with other devices are discussed in Sec. III.

E. Sum- and difference-frequency generation

These processes are described by the Hamiltonian (3) and are distinguished by different initial conditions. For sum-frequency generation one has $\langle n_a \rangle_{\text{in}} = 0$, and the number of photons created at the sum frequency ω_a is equal to the number of photons annihilated at each of the two source frequencies ω_b and ω_c. For difference-frequency generation, on the contrary, $\langle n_b \rangle_{\text{in}} = \langle n_c \rangle_{\text{in}} = 0$ and the number of photons created at each of the two difference frequencies $\omega_{b,c}$ is equal to the number of photons annihilated at the source frequency ω_a.

Hamiltonian (3) has the following constants of motion:

$$\hat{S} = \frac{1}{2}\left(2a^\dagger a + b^\dagger b + c^\dagger c\right) \,, \tag{26}$$

$$\hat{D} = b^\dagger b - c^\dagger c \,. \tag{27}$$

The Hilbert subspace of interest for applications is that corresponding to the eigenvalue $D = 0$. The subspaces for fixed eigenvalues S are spanned by the eigenvectors

$$|n\rangle_S = |n, S-n, S-n\rangle \,, \tag{28}$$

and for fixed S the Hamiltonian (3) takes the tridiagonal form

$$\hat{H}|n\rangle_S = h_n^{(S)}|n-1\rangle_S + h_{n+1}^{(S)}|n+1\rangle_S \,, \tag{29}$$

$$h_n^{(S)} = \sqrt{n}(S-n+1) \,. \tag{30}$$

The evolution of the field has been evaluated through numerical diagonalization (as a check, numerical results presented in Refs. [18, 1] have been reproduced).

The gain and output Fano factor for input number eigenstates are plotted in Fig. 4 (the gain is defined with respect to only one of the two subharmonic modes). The results obtained are qualitatively similar to those for second- and subharmonic generation: complete conversion is never achieved and sum-frequency generation is more efficient than difference-frequency generation. The gain $\mathcal{G}$ for difference-frequency generation is a decreasing function of the input signal, and asymptotically $\mathcal{G} = 0.78$. The corresponding Fano factor is an increasing (almost linear) function of the input photon number; hence, the duplication performance (photon splitting) is far from being ideal for large signals.

Sum-frequency generation, contrarily to the difference-frequency case, achieves ideal gain $\mathcal{G} = 1$ for large signals, whereas the Fano factor decreases versus signal and tends

asymptotically to the same value $\mathcal{F}_{out} = 0.13$ achieved by the second-harmonic generation. Thus, very good performances can be expected for sum-frequency generation at large signals. The noise figure and gains for input coherent states reflect analogous behaviors to second and subharmonic generation, and are not reported here.

III. DISCUSSION

We have analyzed the gain and noise-figure of the trilinear parametric processes for direct detection. The problem of second- and subharmonic and sum- and difference-frequency generation has been solved through direct diagonalization, which is the most reliable method for such nonlinear processes (for an introduction to alternative methods, see Ref. [19]). Because the Manley-Rowe relations lead to integrals of motion, the diagonalization problem is reduced to a finite-dimensional subspace. After performing the diagonalization numerically, we ana-
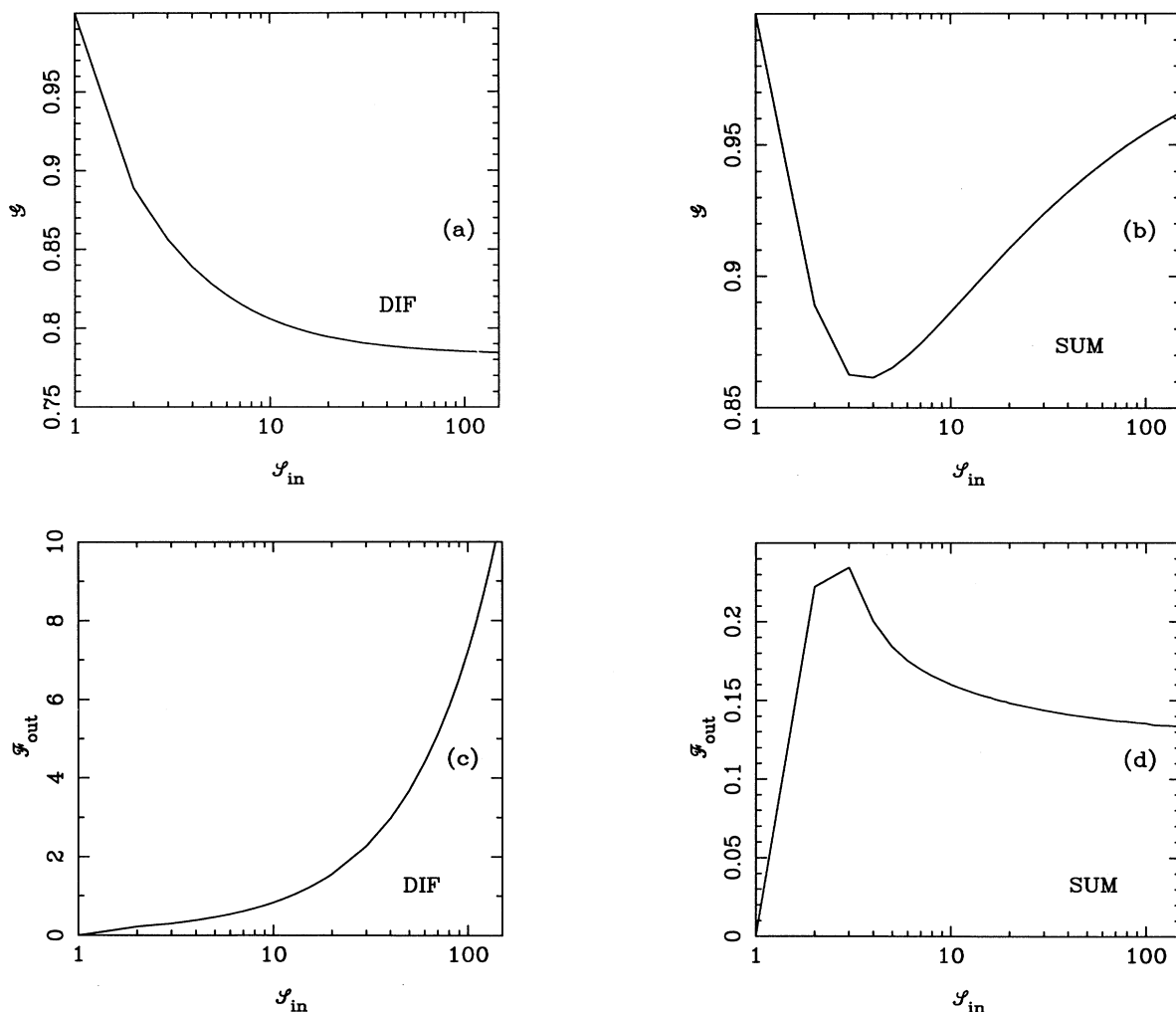

FIG. 4. Same as in Fig. 2 for the nondegenerate case, i.e., difference-frequency and sum-frequency generation [Hamiltonian (3)].

lyzed the processes for input number states as well as for coherent superpositions. We showed that the depletion of the quantum pump is never complete and the unconverted photons account for additional noise at the output: this phenomenon is the parametric counterpart of the customary spontaneous emission that occurs in the nonparametric processes (and is usually termed *spontaneous parametric emission* [20]). A comparison of the frequency generation processes shows that second-harmonic and sum-frequency generation are more efficient than the respective down-conversion processes: the former achieve ideal gains and low output noise for high input signals, the latter exhibit gains below the ideal values, whereas the noise figures increase with the input signals. Thus, due to spontaneous parametric emission and contrarily to what was suggested in Ref. [14], subharmonic generation does not attain the gain $\mathcal{G} = 2$ number amplification, and, analogously, difference frequency does not perform as an ideal photon-number duplicator.

In Figs. 2(c), 2(d) and 3(c), 3(d) the output noises of the frequency generation processes are compared with those of the customary phase-sensitive and insensitive amplifiers operating at the same gain: such a parallel analysis is interesting for applications using these devices in cascades. For input number states the best performance is achieved by the phase-insensitive amplifier, whereas for input coherent states by the phase-sensitive, the latter being essentially ideal for high input signals (taking into account the saturation effects would lead to improved noise figures for the phase-insensitive amplifier working at such low gains [5]). Subharmonic generation is the most noisy process for both coherent and number input states, whereas second-harmonic generation is better than the phase-insensitive amplification, and even better than the phase-sensitive for low input signals.

ACKNOWLEDGMENTS

* Electronic address: DARIANO@PV.INFN.IT

† Electronic address: MACCHIAVELLO@PV.INFN.IT

[1] G. Drobný and I. Jex, Phys. Rev. A **46**, 499 (1992).

[2] R. Loudon and T. J. Shepherd, Opt. Acta **31**, 1243 (1984).

[3] R. Loudon, IEEE J. Quantum Electron. **QE-21**, 766 (1985).

[4] Y. Yamamoto and T. Mukai, Opt. Quantum. Electron. **21**, S1 (1989).

[5] S. Ruiz-Moreno, J. Guitart, and M. J. Soneira, in *Quantum Aspects of Optical Communications*, edited by C. Bendjaballah, O. Hirota, and S. Reynaud, Lecture Notes in Physics 378 (Springer, Berlin, 1991), p. 376.

[6] For a review on quantum communication and detection theory, see the collection of papers quoted in Ref. [5].

[7] P. N. Butcher and D. Cotter, *The Elements of Nonlinear Optics* (Cambridge University Press, Cambridge, 1991).

[8] H. P. Yuen, Opt. Lett. **12**, 789 (1987).

[9] For experimental measurements of noise-figure optical-fiber amplifiers, see M. Artiglia, P. Bonanni, A. Cavaciuti, M. Potenza, M. Puleo, and B. Sordo, *Technical Digest of the Symposium on Optical Fiber Measurements* (NIST, Boulder, CO, 1992).

[10] G. M. D'Ariano, NASA Report No. CP-3135 (1992), p. 311.

[11] G. M. D'Ariano, Phys. Rev. A **45**, 3224 (1992).

[12] G. M. D'Ariano, Int. J. Mod. Phys. B **6**, 1291 (1992).

[13] R. A. Brandt and O. W. Greenberg, J. Math. Phys. **10**, 1168 (1969).

[14] H. P. Yuen, in *Quantum Aspects of Optical Communications* (Ref. [5]).

[15] H. P. Yuen, Phys. Rev. Lett. **56**, 2176 (1986).

[16] R. Tanaś and T. Gantsog, Quantum. Opt. **4**, 245 (1992).

[17] G. M. D'Ariano, C. Macchiavello, and M. Paris, NASA Report No. CP-3219, 1993 (unpublished), p. 71.

[18] D. F. Walls, in *Quantum Optics, Proceedings of the Scottish University Summer School, 10th; Edinburgh 1969*, edited by S. M. Kay and Maitland (Academic, New York, 1970), p. 501.

[19] A. Schenzle, in *New Frontiers in Quantum Electrodynamics and Quantum Optics*, Vol. 232 of *NATO Advanced Study Institute, Series B: Physics*, edited by A. O. Barut (Plenum, New York, 1990), p. 63.

[20] R. Graham, *Quantum Optics* (Ref. [18]), p. 489.